Arash Abbasnia
Mahmoud Ghiasi

ISSN 1333-1124

SIMULATION OF NONLINEAR WAVE INTERACTION WITH DUAL CYLINDERS IN NUMERICAL WAVE TANK

UDC 532.5:519.6

Summary

A fully nonlinear numerical wave tank (NWT) is developed to investigate the interaction of waves and fixed dual cylinders accurately. The potential theory and the mixed Eulerian-Lagrangian (MEL) method are used to solve the time domain multi-boundary problem. The high order boundary element method (BEM) is applied to compute the boundary values in the Eulerian frame. The material node approach combined with the fourth order Runge-Kutta time integration is employed to update the boundary values in the Lagrangian frame. Boundary geometry and tangential derivatives of boundary values are obtained by the Non-Uniform Rational B-spline (NURBS) approximation. The time derivative of velocity potential is calculated by the acceleration potential formulation. Free surface elevation and hydrodynamic forces on the objects evaluated by the present numerical procedure are compared with other numerical simulations.

Key words: *numerical wave tank, MEL, boundary element, wave-body interaction*

1. Introduction

Recently, the use of a numerical wave tank for studying the wave-body interaction in time domain has been of interest in marine hydrodynamics. In the past two decades, numerical wave tanks have been developed to simulate various hydrodynamics problems such as wave interaction with waves, currents, variable bottom and fixed or floating bodies. For the simulation of linear wave-body interaction, the free surface boundary condition was linearized and the solution was obtained in the time and frequency domain by Nakos et al. [16]. Perturbation theory was used for weakly nonlinear problems but it is complicated for higher order problems. Linear and second order wave interaction with a floating body was proposed by Kim et al. [11] based on the diffraction and perturbation theory. Second order wave-current interaction with floating bodies was presented by Liu and Teng [14]. Mixed Eulerian-Lagrangian time marching technique was presented by Longuet-Higgins and Cokelet [15], to solve the fully nonlinear free surface problem. By using this technique, the fully nonlinear free surface boundary conditions can be applied on the exact free surface. In the time stepping approach, free surface boundary values are calculated in the Eulerian frame at each time step and a new position and value of the moving boundary are obtained in the Lagrangian manner

for the next time step. Many attempts have been made to develop NWTs for fully nonlinear modelling of free surface wave problems, such as overturning waves over arbitrary bottom by Grilli et al. [8] and wave-current interaction by Ryu et al. [21]. Studies on propagation of regular and irregular waves were also conducted by Ning and Teng [17], Tang and Huang [22] and Ning et al. [18]. Wave interaction with an array of fixed cylinders was presented by Wang and Wu [27] and wave interaction with free floating bodies was presented by Koo and Kim [12]. To solve the Laplace equation in the potential numerical wave tanks, the BEM and finite elements methods (FEM) were used based on the linear or curvilinear elements by Wu and Hu [28], Wang and Wu [26] and Guerber et al. [10]. B-spline BEM formulations for the continuous boundary problem and boundaries with corner points were provided by Cabral et al. [3], [4]. Indirect NURBS panel method was proposed by Gao and Zou [7] to study linear simulation of uniform motion of submerged subjects. To update the instantaneous computational domain, various time integration schemes such as the fourth order Runge-Kutta method by Koo and Kim [12], the fifth order Runge-Kutta-Gil and the fourth order Adams-Bashforth-Moulton method by Zhang et al. [29] have been developed.

Evaluation of hydrodynamic loads on bodies based on the acceleration potential was reviewed by Bandyk and Beck [1]. The formulation was firstly introduced by Vinje and Brevig [25] in which a potential wave-body problem is solved in a complex domain. For a fixed body, the backward finite difference formula is the simplest way to approximate the potential change in time but spike instability might occur for incident nonlinear large amplitude wave. Tanizawa [23] presented a formulation for the calculation of time derivative of the potential for a freely floating body problem.

In this paper, a fully nonlinear two dimensional potential NWT is developed based on the NURBS BEM and the acceleration potential to solve the time dependent boundary value problem of linear wave interaction with dual cylinders. An artificial wavemaker is deployed on the upstream fixed end wall by specifying normal flux of the linear potential wave theory. To reduce the wave reflection into the computational domain, two numerical wave absorbers are set on the specified length of the free surface at the rear of the downstream end wall and in front of the upstream end wall. Hence, a viscous damping coefficient proposed by Cointe [6] is added to the fully nonlinear free surface boundary conditions. The fourth order Runge-Kutta time integration and the MEL method are used for time stepping and the Gauss quadrature integration scheme is applied to determine hydrodynamic forces. Free surface elevation and hydrodynamic forces obtained by the present numerical procedure are compared with former studies. Coupling of boundary geometry description by the NURBS and direct BEM in NWTs can be a novel numerical procedure to evaluate boundary values and their derivatives.

2. Mathematical Model

The computational domain Ω is illustrated in Figure 1. A Cartesian coordinates system Oxz is chosen such that positive z is upwards and the origin is located on the still water level. It is assumed that the fluid is homogenous, incompressible and inviscid and the flow is irrotational. Hence, the governing equation of the velocity potential ϕ can be written as:

$$\nabla^2\phi = 0 \quad \text{in } \Omega(t) \tag{1}$$

To solve the boundary value problem, fully nonlinear kinematics free surface boundary condition (KFSBC) and fully nonlinear dynamics free surface boundary condition (DFSBC) are applied on the exact free surface Γ_5;

$$\begin{aligned} &\frac{\partial \eta}{\partial x}=\frac{\partial \phi}{\partial z}-\frac{\partial \phi}{\partial x}\frac{\partial \eta}{\partial x} \ \text{(KFSBC)} \\ &\frac{\partial \phi}{\partial t}=-gz-\frac{1}{2}\left|\nabla \phi\right|^2 \ \text{(DFSBC)} \end{aligned} \quad \text{on } \Gamma_5 \tag{2}$$

where, $\eta(x,t)$ is the wave elevation measured from the still water level, and g is the gravitational acceleration. In terms of the Lagrangian manner based on the material node approach, the fully nonlinear free surface boundary conditions can be written as:

$$\begin{aligned} &\frac{\delta \phi}{\delta t}=-g\eta+\frac{1}{2}\left|\nabla \phi\right|^2 \\ &\frac{\delta \vec{X}}{\delta t}=\nabla \phi \end{aligned} \tag{3}$$

where $\delta/\delta t=\partial/\partial t+\vec{\upsilon}.\nabla$ in which $\vec{\upsilon}=\nabla\phi$ and $\vec{X}$ is the location of free surface nodes.

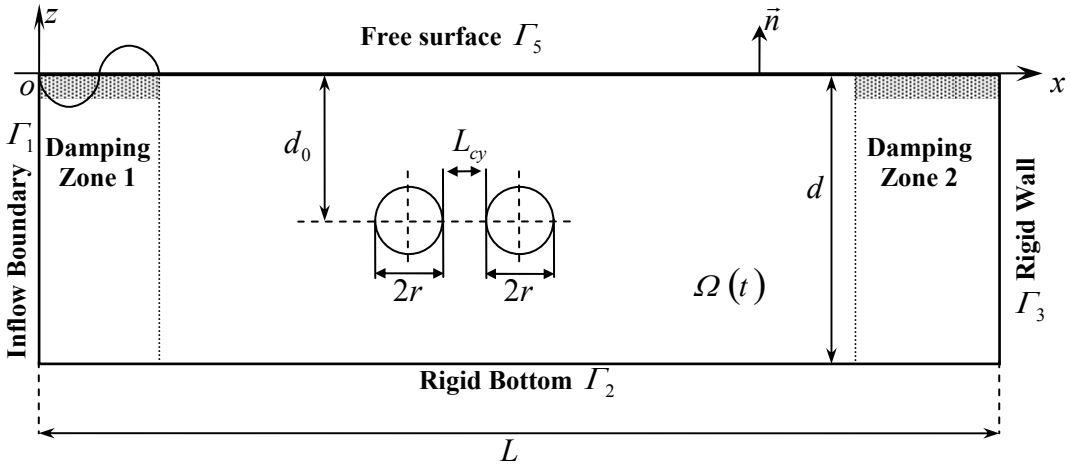

Fig. 1 Definition sketch of numerical wave tank

The condition on the fixed upstream end wall Γ_1 (inflow boundary) is given as:

$$\frac{\partial \phi}{\partial n}=-\frac{\partial \phi_w}{\partial x} \quad \text{on } \Gamma_1 \tag{4}$$

where, ϕ_w could be the linear or nonlinear wave potential. Impermeable conditions on the bottom Γ_2, downstream end wall Γ_3 and body surface Γ_4 are given as:

$$\frac{\partial \phi}{\partial n}=0 \ \text{ on } \Gamma_2, \Gamma_3 \text{ and } \Gamma_4 \tag{5}$$

To achieve an appropriate numerical solution for the wave-body interaction problem in a numerical wave tank, the use of artificial damping zones (sponger layer) is inevitable at both ends of the wave tank. An artificial damping term is added to the free surface boundary condition on the specific length of the free surface at the adjacent of the end walls. Cointe [6] presented the numerical wave absorber as:

$$\begin{aligned} \frac{\delta \vec{X}}{\delta t} &= \nabla\phi - \nu(x)\left(\vec{X} - \vec{X}_e\right) \\ \frac{\delta \phi}{\delta t} &= -g\eta + \frac{1}{2}\left(\nabla\phi.\nabla\phi\right) - \nu(x)\left(\phi - \phi_e\right) \end{aligned} \quad \text{on } \Gamma_5 \tag{6}$$

where, the subscript e corresponds to the reference configuration of the fluid. The function $\nu(x)$ is the damping coefficient defined as:

$$\nu(x) = \alpha\omega\left[\frac{K}{2\pi}(x - x_0)\right]^2 \ , \ x_0 \le x \le x_1 = x_0 + \frac{2\pi\beta}{K} \tag{7}$$

In practice, the damping coefficient is equal to zero except in the damping zone $(x_0 \le x \le x_1)$, which is tuned to a characteristic wave frequency ω and to a characteristic wave number K. Strength and length of the damping zone are controlled by the dimensionless parameters α and β, respectively. The terms ϕ_e and $\vec{X}_e = (x_e, z_e)$ are reference values. When reference values are set as calm water condition $(\phi_e$ and $z_e = 0)$, the damping zone acts as a simple absorber.

3. NURBS Boundary Element Method

3.1 Non-Uniform Rational B-spline Curve

To solve the boundary value problem, the geometry description of boundary is substantial particularly for the complicated deformation boundary. Piegl and Tiller [20] summarized the parametric interpolation functions such as Bezier, B-spline, and Non-Uniform Rational B-spline curve (or surface). The NURBS curve is a piecewise function, given as:

$$\vec{X}(u) = (x(u), z(u)) = \frac{\sum_{i=1}^{m} N_i^{(p)}(u)\vec{P}_i w_i}{\sum_{i=1}^{m} N_i^{(p)}(u) w_i} \tag{8}$$

where, $0 \le u \le 1$ is the parametric value of the B-spline curve, m is the number of control points $\vec{P}_i$, $N_i^{(p)}$ is the B-spline basis function with a degree of p, and w_i is the weighted function. Inflection of the free surface and submerged bodies can be approximated accurately by a parametric curve to obtain geometry characteristics such as normal vector, length and calculating spatial derivation of boundary values. Equation (8) provides a system of m linear equations for the known curve point χ_k and the unknown control points. It can be written as:

$$\sum_{i=1}^{m} \Re_i^{(p)}(\bar{u}_k)\vec{P}_i = \chi_k \ , \ k = 1,...,m \tag{9}$$

in which,

$$\Re_i^{(p)}(u) = \frac{N_i^{(p)}(u) w_i}{\sum_{j=0}^{m} N_j^{(p)}(u) w_j} \tag{10}$$

Using $\bar{u}_k$ the value of knots, the m values of rational functions $\Re_1^{(p)},...,\Re_m^{(p)}$ are computed, and the position of control points is then obtained. $\bar{u}_k$ is given as;

$$\bar{u}_k = \bar{u}_{k-1} + \frac{\left|\chi_k - \chi_{k-1}\right|}{q}\ ,\ k = 2,...,m-1 \tag{11}$$

where $q = \sum_{k=1}^{m} \left|\chi_k - \chi_{k-1}\right|$.

To solve the boundary integral equation, the boundary points are selected on the free surface and the corresponding terms of the points are computed based on the NURBS description of the free surface.

The unit tangent vector $\vec{s}$ for any collocation point in the u direction is defined as:

$$\vec{s} = s_x\vec{i} + s_z\vec{k} = \frac{\vec{T}_u}{\left|\vec{T}_u\right|} \tag{12}$$

in which $\vec{T}_u = \left(\partial x/\partial u\,, \partial z/\partial u\right)$ is tangential vector along the u direction. The unit normal vector is written as:

$$\vec{n} = \frac{-\dfrac{\partial z}{\partial u}\vec{i} + \dfrac{\partial x}{\partial u}\vec{k}}{\left|\vec{T}_u\right|} \tag{13}$$

3.2 Boundary Integral Equation for Multi-Boundary Problem with Corner Point

The boundary integral equation based on the Green second identity is employed to solve the multi-boundary value problem. It is written as:

$$c_i\phi_i + \int_\Gamma \phi\left(\vec{X}\right)\frac{\partial G}{\partial n}\left(\vec{X}, \vec{X}_i\right)d\Gamma = \int_\Gamma G\left(\vec{X}, \vec{X}_i\right)\frac{\partial \phi}{\partial n}\left(\vec{X}\right)d\Gamma \tag{14}$$

where $c_i = \theta_i/2\pi$, θ_i is the internal angle at node i on the integrating boundary Γ of the computational domain which is enclosed by the internal boundary (Γ_4) and the external boundaries ($\Gamma_1 \cup \Gamma_2 \cup \Gamma_3 \cup \Gamma_5$). For two dimensional problems, the Green function is

$$G\left(\vec{\mathrm{X}}, \vec{\mathrm{X}}_i\right) = -\frac{1}{2\pi}\ln R \tag{15}$$

where

$$R = \left|\vec{\mathrm{X}} - \vec{\mathrm{X}}_i\right| \tag{16}$$

is the distance from the field point $\vec{X}$ to the source point $\vec{X}_i$. In this study, the inflow wall, the end wall and the bottom can be described exactly by the linear shape function. The position of the nodal points on the free surface and on the surface of submerged bodies can be obtained by the NURBS curve. Therefore, the variation of the geometry and boundary values over boundary l is described as:

$$\vec{X}^l = \sum_{j=1}^{N_l} B_j^l(u)\vec{X}_j^l \tag{17}$$

$$\phi^l = \sum_{j=1}^{N_l} B_j^l(u)\phi_j^l \tag{18}$$

$$\frac{\partial \phi^l}{\partial n} = \sum_{j=1}^{N_l} B_j^l(u) \frac{\partial \phi_j^l}{\partial n} \tag{19}$$

in which $l = 1,2,...,5$ and N_l and $B_j^l(u)$ are the number of nodes and the local shape function corresponding to the boundary l, respectively. $\vec{X}_j^l$, ϕ_j^l and $\partial \phi_j^l / \partial n$ are geometry, potential and its normal flux of the node j on the boundary l, respectively. For total points on the boundaries ($N = N_1 + N_2 + N_3 + N_4 + N_5$), the integrals of Equation (14) can be discretized as:

$$\int_\Gamma \phi \frac{\partial G_i}{\partial n} d\Gamma = \sum_{l=1}^{5} \sum_{j=1}^{N_l} \phi\left(\vec{X}_j^l\right) \int_{\Gamma_l} B_j^l(u) \frac{\partial G\left(\vec{X}^l(u), \vec{X}_i\right)}{\partial n} J^l(u) du = \sum_{l=1}^{5} \sum_{j=1}^{N_l} F_{ij}^l \phi_j^l \tag{20}$$

$$\int_\Gamma G_i \frac{\partial \phi}{\partial n} d\Gamma = \sum_{l=1}^{5} \sum_{j=1}^{N_l} \frac{\partial \phi}{\partial n}\left(\vec{X}_j^l\right) \int_{\Gamma_l} B_j^l(u) G\left(\vec{X}^l(u), \vec{X}_i\right) J^l(u) du = \sum_{l=1}^{5} \sum_{j=1}^{N_l} E_{ij}^l \frac{\partial \phi_j^l}{\partial n} \tag{21}$$

where the Jacobian is defined as:

$$J^l = \sqrt{\left(\frac{dx^l}{du}\right)^2 + \left(\frac{dz^l}{du}\right)^2} \tag{22}$$

and F_{ij}^l denotes the array of the Dirichlet matrix and E_{ij}^l is the array of the Neumann matrix. There are four corner points at the intersection of the inflow wall and the end wall with the bottom and the free surface. The double point approach proposed by Brebbia and Domingues [2] is used to treat the potential normal flux discontinuity of boundary values. Since, the potential is unique at any boundary point, but the potential flux is not unique because the normal vector on the boundary at the intersection point is not sole and the flux differs before and after the corner point. The condition on the moving corner points on the free surface is given in Figure 2 (Case 1). At these corner points the potential and normal flux on the one side of the points are known and on the other side are unknown. For the fixed corner points on the bottom (Case 2), the fluxes on both sides are known but the potentials are unknown values.

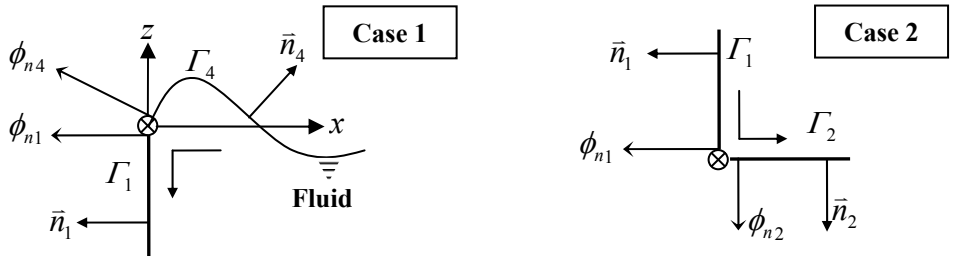

Fig. 2 Magnified view of intersection points ($\otimes$) boundary values

Substituting Equations (20) and (21) into Equation (14), the discretized form of Equation (14) can be written as:

$$c_i \phi_i = \sum_{l=1}^{5} \sum_{j=1}^{N_l} \left\{ E_{ij}^l \frac{\partial \phi_j^l}{\partial n} - F_{ij}^l \phi_j^l \right\} \tag{23}$$

in which $i = 1, \cdots, N$. By moving the unknown value to the left-hand side (LHS) of Equation (23) and the known values to the right-hand side (RHS) of the equation, Equation (23) can be written as:

$$\sum_{j=1}^{N_5} E_{ij}^5 \frac{\partial \phi_j^5}{\partial n} - \sum_{l=1}^{4}\sum_{j=1}^{N_l} \overline{F}_{ij}^l \phi_j^l = \sum_{l=1}^{4}\sum_{j=1}^{N_l} E_{ij}^l \frac{\partial \overline{\phi}_j^l}{\partial n} - \sum_{j=1}^{N_5} \overline{F}_{ij}^5 \overline{\phi}_j^5 \tag{24}$$

where $\overline{\phi}_j^l$ and $\partial \overline{\phi}_j^l / \partial n$ are the known boundary values. $\overline{F}_{ij}^l$ is equal to $c_i + F_{ij}^l$ if i coincides with the boundary points, otherwise $\overline{F}_{ij}^l$ is equal to F_{ij}^l. By solving the system of equation, the unknown values are obtained and the moving computational domain is updated and regridded.

4. Time Stepping Scheme

At every time step, the velocity and time derivative of the potential of the free surface nodes are computed. Normal flux of the free surface potential and its tangential derivative are obtained by the boundary integral solution and the NURBS scheme, respectively. Spatial derivative of the free surface potential in the Cartesian coordinates can be written as:

$$\begin{Bmatrix} \frac{\partial \phi}{\partial x} \\ \frac{\partial \phi}{\partial z} \end{Bmatrix} = \begin{bmatrix} \frac{\partial x}{\partial s} & -\frac{\partial z}{\partial s} \\ \frac{\partial z}{\partial s} & \frac{\partial x}{\partial s} \end{bmatrix} \begin{Bmatrix} \frac{\partial \phi}{\partial s} \\ \frac{\partial \phi}{\partial n} \end{Bmatrix} \tag{25}$$

where $\partial x/\partial s$ and $\partial z/\partial s$ is approximated by the NURBS curve along the curvilinear coordinates.

To obtain the velocity of corner points 1 and 4 the double nodes approach is used. Points 1 and 4 are located at the intersection of the free surface and the inflow and outflow boundaries, respectively. Each corner point on the free surface has a unique velocity in the Cartesian coordinate system. To evaluate the tangential derivative of the potential at the corner points the formula proposed by Grilli and Svendsen [9] is used:

$$\frac{\partial \phi^5}{\partial s} = \frac{\partial \phi^5}{\partial n} \frac{\cos(\theta_m - \theta_5)}{\sin(\theta_m - \theta_5)} - \frac{\partial \phi^m}{\partial n} \frac{1}{\sin(\theta_m - \theta_5)} \tag{26}$$

in which $m = 1$ and $m = 3$ correspond to the inflow boundary and the outflow boundary, respectively. θ_5 is the devitation angle of the free surface nodal points;

$$\tan(\theta_5) = \frac{\partial z}{\partial x} \tag{27}$$

For the inflow boundary $\theta_1 = \pi/2$ and for the end wall $\theta_3 = 3\pi/2$. $\partial \phi^5 / \partial n$ and $\partial \phi^m / \partial n$ are the potential normal flux at the corner points on the free surface and the inflow boundary or the end wall, respectively. Having velocity of the free surface node, the time derivative of the potential is obtained by the fully nonlinear dynamic free surface boundary condition. The fourth order Rung-Kutta time integration scheme is applied to update the position and potential of the nodes.

5. Acceleration Potential Theory

For computation of pressure and force on the submerged bodies, the time derivative of the potential should be calculated accurately. The simplest approach is the backward difference method for calculation of the time derivative of the potential at each time step. However, for a nonlinear problem this method is unstable in most cases.

The boundary integral equation can be used to calculate the acceleration field. Indeed, its gradient shows fluid particle acceleration. Since $\partial\phi/\partial t$ satisfies the Laplace equation, it can be obtained by solving the integral equation in the computational domain. The time derivatives of the potential can be obtained from the following integral equation.

$$c_i \frac{\partial \phi_i}{\partial t} = \int_\Gamma \left(G_i \frac{\partial^2 \phi}{\partial t \partial n} - \frac{\partial \phi}{\partial t} \frac{\partial G_i}{\partial n} \right) d\Gamma \tag{28}$$

The acceleration potential boundary integral equation can be solved similarly to Equation (14) with the following boundary conditions:

1. The boundary condition on the inflow boundary:

$$\frac{\partial^2 \phi}{\partial n \partial t} = -\frac{\partial^2 \phi_w}{\partial x \partial t} \quad \text{on } \Gamma_1 \tag{29}$$

2. The bottom, outflow and body surface boundary conditions:

$$\frac{\partial^2 \phi}{\partial n \partial t} = 0 \quad \text{on } \Gamma_2, \Gamma_3 \text{ and } \Gamma_4 \tag{30}$$

3. The free surface boundary condition:

$$\frac{\partial \phi}{\partial t} = -gz - \frac{1}{2}\left|\nabla \phi\right|^2 \quad \text{on } \Gamma_5 \tag{31}$$

6. Numerical Application and Results

6.1 Fully Nonlinear Wave Interaction with Single Submerged Cylinder

The present developed potential NWT is based on the NURBS multi-boundary integral equation and the acceleration potential theory is first used to obtain the nonlinear wave force on a fixed submerged circular cylinder. The numerical results are compared with the theoretical solutions of Ogilvie [19], the experimental measurements of Chaplin [5] and the numerical studies of Koo et al. [13]. The mean vertical forces are calculated and compared in Figure 3. The tank length $L = 6m$, tank depth $d = 0.85m$, damping zone 1 has $\alpha = 0$ and damping zone 2 has $\alpha = 1, \beta = 2$. The linear theoretical wave potential is used as feeding input velocity:

$$\phi_w = \frac{gA}{\omega} \frac{\cosh\left[K(d+z)\right]}{\cosh(Kd)} \sin(Kx - \omega t) \tag{32}$$

where A is the wave amplitude. Mesh size and time step are chosen $\Delta x = \lambda/40$ and $\Delta t = T/30$, where $\lambda = 2\pi/K$ and $T = 2\pi/\omega$. The cylinder diameter is $2r = 0.102m$ and $d_0 = 2r$.

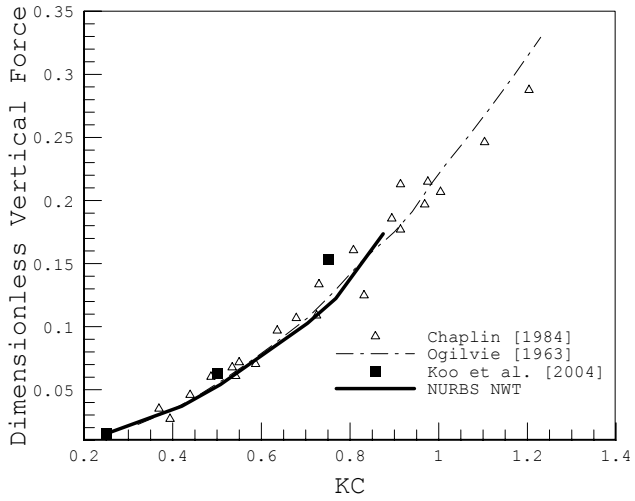

Fig. 3 Dimensionless mean vertical forces $\left(F_v/\rho\omega^2 r^3\right)$ versus Keulegan-Carpenter number

It is shown that the present results are in good agreement with the experimental data and the theoretical solution for various Keulegan-Carpenter numbers $KC = \pi A e^{-Kd_0}/r$. The slight discrepancy between the experimental results and the numerical solution results from viscous effects. First harmonic components of the horizontal force amplitudes are compared analogously in Figure 4.

It seems that the fluid viscosity causes significant differences between the experimental measurement and the potential-based results for large KC. The present results are in good agreement with the high-order theoretical and numerical calculations. Figure 3 and 4 show that the viscosity effect on the computation of vertical forces is negligible in comparison to its effect on horizontal forces.

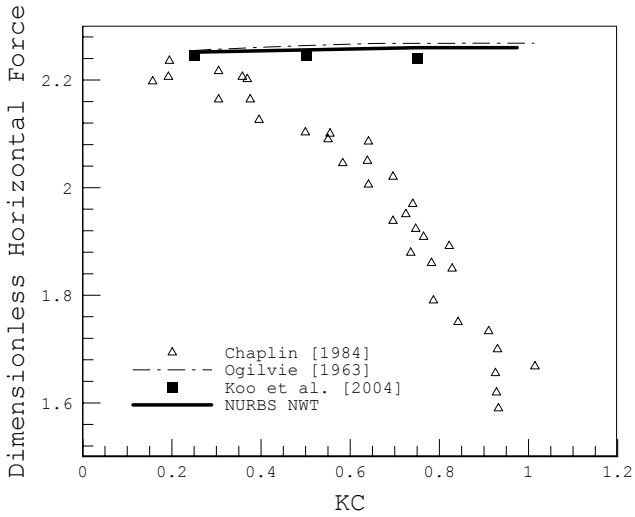

Fig. 4 Dimensionless amplitude of horizontal forces $\left(F_h/\rho\omega^2 r^3\right)$ versus Keulegan-Carpenter number

Time series of vertical and horizontal forces (without the hydrostatic force) on the cylinder in the NURBS NWT is illustrated for $KC = 0.5$ in Figure 5. A snapshot of pressure distribution over the cylinder is shown in Figure 6 at $t = 6.33s$.

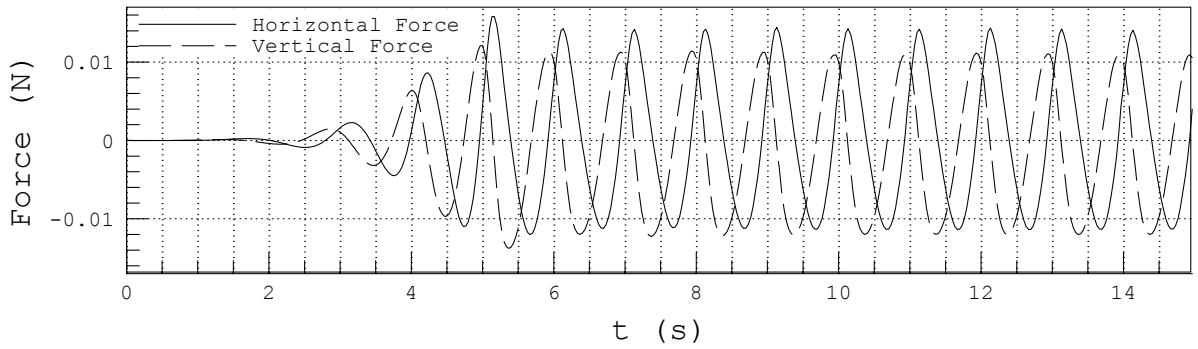

Fig. 5 Time series of horizontal and vertical forces on submerged cylinder

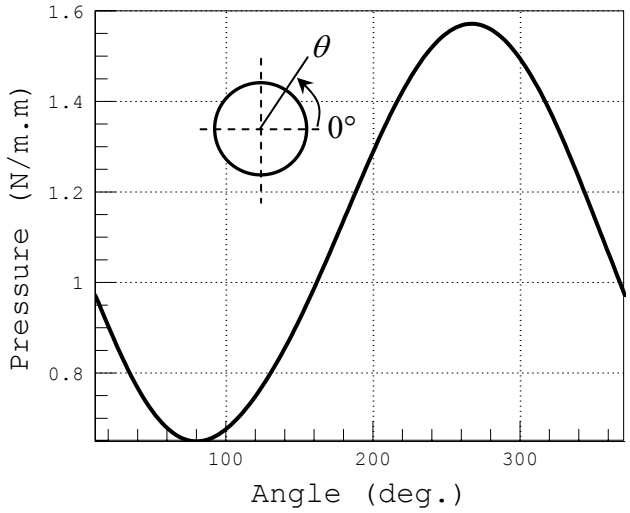

Fig. 6 A snapshot of pressure distribution over the body

Asymmetric pressure distribution on the LHS and the RHS of the cylinder is due to horizontal forces. Free surface wave is depicted for various KC numbers in a snapshot of the whole length of the tank in Figure 7 at $t = 6.67s$. The cylinder diameter is $2r = 0.2m$ with $d_0 = 0.2m$ and the input wave with $\omega = 6.6s^{-1}$ is generated through the NWT with $L = 6\lambda$. Also, the cylinder is located a wave length (λ meter) in front of the inflow boundary. Damping zone 1 vanishes and the damping zone 2 parameters are chosen $\alpha = 1, \beta = 2$. The pressure distribution over the body is shown in Figure 8.

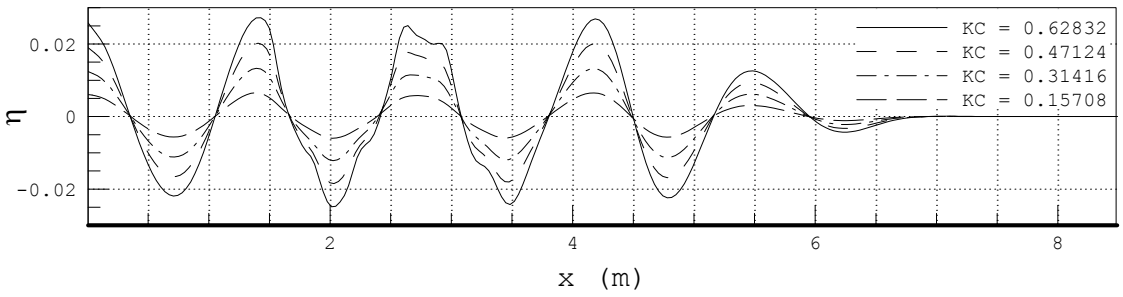

Fig. 7 Spatial series of wave elevation in presence of submerged cylinder for various KC

Figure 7 shows the damping zone 2 performance for various KC numbers and the input wave height. Deformation in the wave profile behind the cylinder is noticeable and increases by increasing the wave height and KC. The vertical plan symmetric pressure distribution

shown in Figure 8 indicates that the horizontal force is zero and the vertical force has maximum value at the instant.

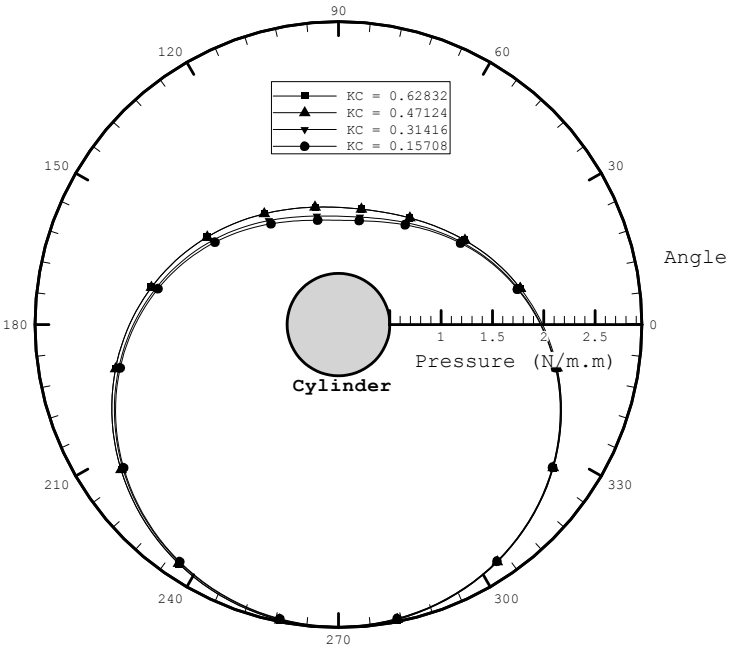

Fig. 8 Pressure distribution on cylinder body for various KC

6.2 Fully Nonlinear Wave Interaction with Dual Submerged Cylinder

In this section, the variation of nonlinear wave forces on two submerged cylinders against different gap distances L_{cy} is presented. Figure 9 shows spatial series of the wave profile in which diameters of both cylinders are taken $0.15m$ and the input wave length is $1.558m$. Depth of the NWT is chosen $0.85m$, its length is 6λ, $\alpha = 1, \beta = 1$ for damping zone 1 and $\alpha = 1, \beta = 2$ for damping zone 2. The first cylinder is located 1.5λ from the inflow boundary and $KC = 0.56$. Mesh size and time step values are similar to the previous subsection. It is shown that more deformation on the wave profile occurs when the gap distance becomes smaller.

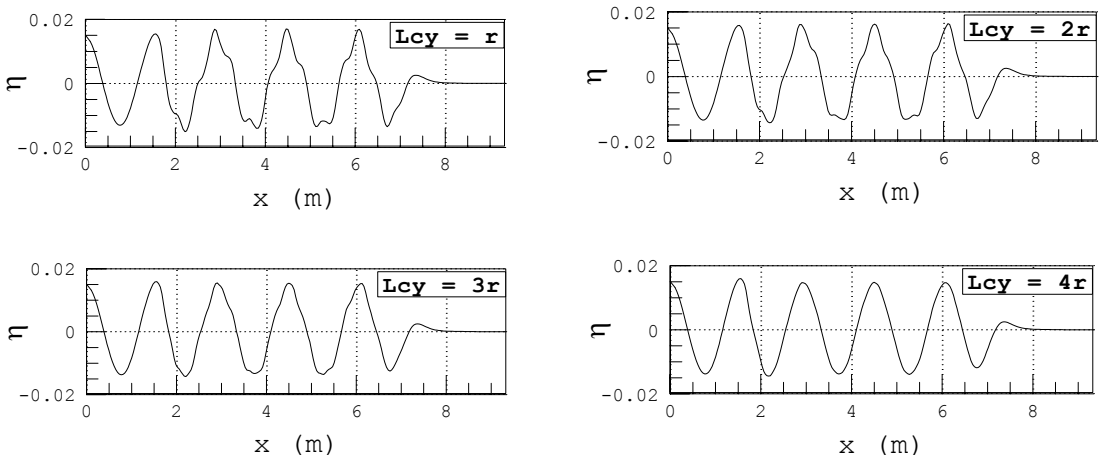

Fig. 9 A snapshot of wave profile in presence of dual cylinders with various L_{cy}

A comparison of pressure distribution over the cylinders for different gap distances is shown in Figure 10 at the same moment.

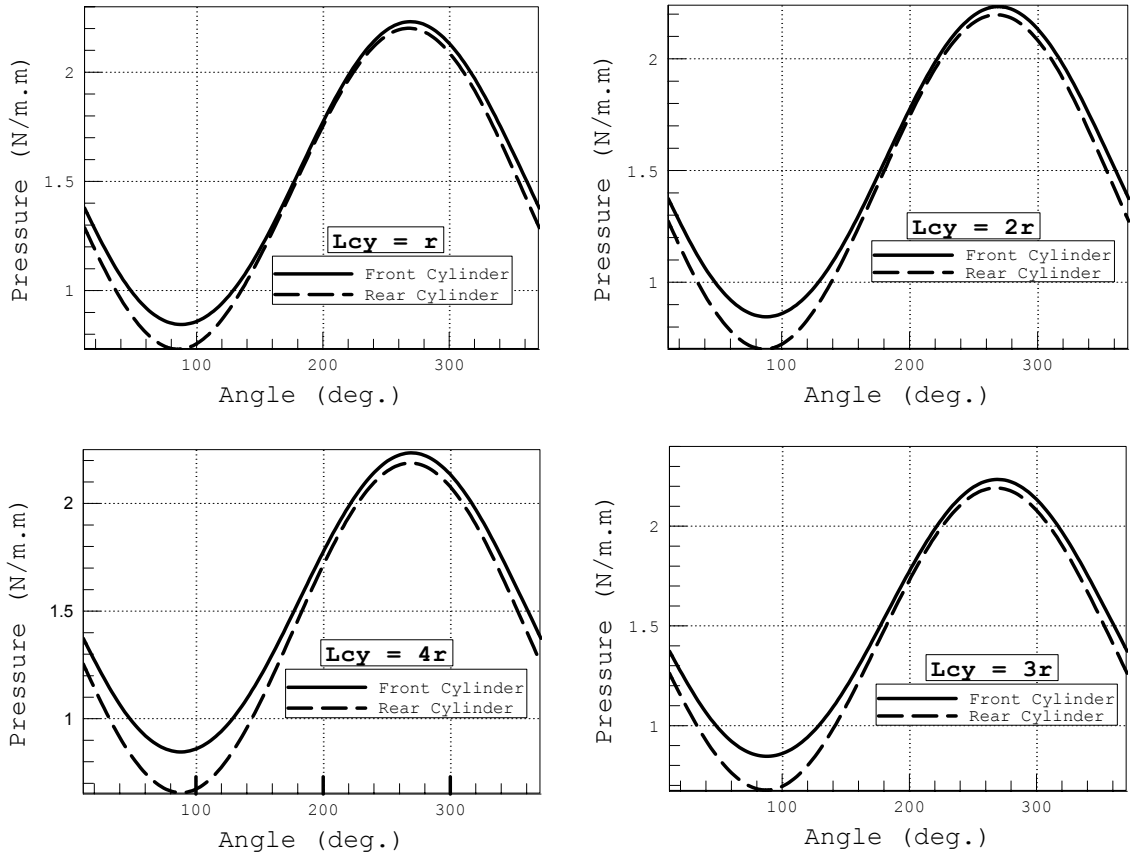

Fig. 10 A snapshot of pressure distribution in presence of dual cylinders with various L_{cy}

It is shown that when the gap distance is larger, the pressure difference between the front cylinder and the rear cylinder becomes greater. Indeed, the rear cylinder undergoes larger forces when the gap distance becomes smaller as shown in Figure 11 and 12. The obtained vertical and horizontal mean forces on the front and rear cylinders are compared with the viscous NWT developed by Tavassoli and Kim [24] and the potential NWT presented by Koo et al. [13].

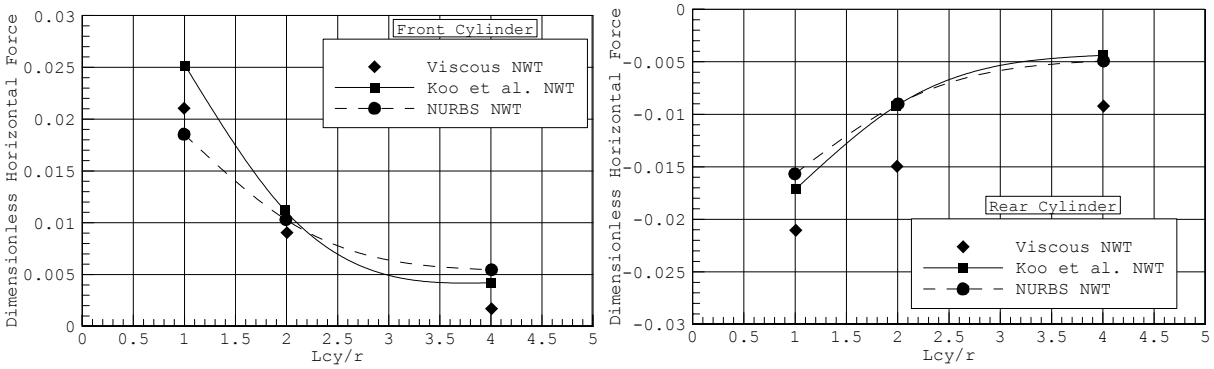

Fig. 11 Mean horizontal force on two cylinders normalized by $\rho\omega^2 r^3$ for various L_{cy}

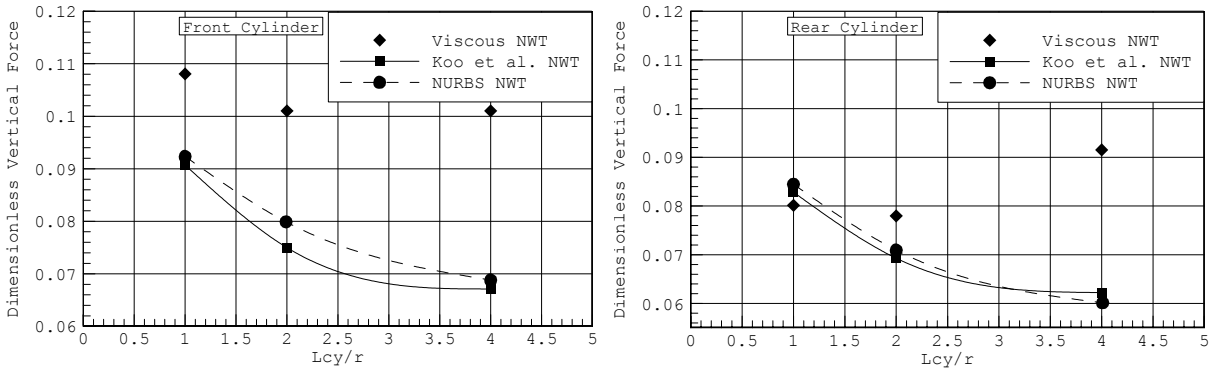

Fig. 12 Mean vertical force on two cylinders normalized by $\rho\omega^2 r^3$ for various L_{cy}

Figure 11 shows that mean horizontal forces on the cylinders are in opposite directions. Hence, two cylinders tend to drift and decrease the gap distance. Also, when the gap distance becomes smaller, this phenomenon severely occurs. In both Figures 11 and 12, trends of the viscous NWT results are the same with the potential solutions.

7. Conclusion

A fully nonlinear two dimensional potential NWT is developed based on the MEL approach and the NURBS boundary element method. Acceleration potential field is used to evaluate hydrodynamic forces on the bodies. Two numerical beaches by adding the artificial damping coefficient to both kinematic and dynamic free surface conditions are set, and their performances are obtained. Wave distortion, pressure distribution and time series of forces due to a fully submerged single cylinder are evaluated and validated by Ogilvie's theoretical solutions and Koo's et al. numerical results and Chaplin's experimental measurements. The substantial difference in wave forces for higher KC numbers seems to be due to the fluid viscosity. The fully nonlinear NURBS NWT is also used to solve a wave interaction problem with fixed dual submerged cylinders by means of the acceleration potential theory for various gaps. It is recognized that the interaction effects are more important when the gap distance becomes smaller. The direction of horizontal forces on the dual cylinders is opposite and two cylinders tend to drift in the opposite direction to reduce the gap. The magnitude of mean horizontal and vertical forces significantly increases when the gap distance decreases.

Acknoledgement

Authors would like to thank the reviewers for their valuable comments.

REFERENCES

[1] P.J. Bandyk, R.F. Beck: *The acceleration potential in fluid-body interaction problems*. J. Eng. Math. 70, 147-163 (2011).

[2] C.A. Brebbia, J. Dominguez: *Boundary elements: An introductory course*. 2nd ed. WIT Pree, UK (Southampton) 1992.

[3] J.J.S.P. Cabral, L.C. Worbel, C.A. Brebbia: *A BEM formulation using B-splines: I- Uniform blending function*. Eng. An. Bound. El. 7(3), 136-144 (1990).

[4] J.J.S.P. Cabral, L.C. Worbel, C.A. Brebbia: *A BEM formulation using B-splines: II- Multiple knots and non-uniform blending function*. Eng. An. Bound. El. 8(1), 51-55 (1991).

[5] J.R. Chaplin: *Nonlinear forces on a horizontal cylinder beneath waves*. J. Fluid Mech. 147, 449–464 (1984).

[6] R. Cointe: *Numerical simulation of a wave channel*. Eng. An. Bound. El. 7(4), 167-177 (1990).

[7] Z.L. Gao, Z.J. Zou: A three-Dimensional Desingularized High order panel method based on NURBS. J. Hydro. 20(2), 137-146 (2008).

[8] S.T. Grilli, P. Guyenne, F. Dias: *A fully non-linear model for three-dimensional overturning waves over arbitrary bottom*. Int. J. Numer. Mech. Fluids. 35, 829-867 (2001).

[9] S.T. Grilli ST, I.A. Svendsen: *Corner problems and global accuracy in the boundary element solution of nonlinear wave flows*. Eng. An. Bound. El. 7(4), 178-195 (1990).

[10] E. Guerber, M. Benoit, S.T. Grilli. *A fully nonlinear implicit model for wave interactions with submerged structures in forced or free motion*. Eng. An. Bound. El. 36, 1151-1163 (2012).

[11] M.H. Kim, M.S. Celebi, D.J. Kim: *Fully nonlinear interactions of waves with a three-dimensional body in uniform currents*. Appl. Ocean Res. 20, 309-321 (1998).

[12] W. Koo, M.H. Kim: *Freely floating-body simulation by a 2D fully nonlinear numerical wave tank*. Ocean Eng. 31, 2011–2046 (2004).

[13] W. Koo, M.H. Kim, A. Tavassoli: *Fully nonlinear wave-body interactions with fully submerged dual cylinders*. Int. J. Offshore Polar Eng. 14, 210–217 (2004).

[14] Z. Liu, B. Teng: *Wave-Current Interactions with Three-Dimensional Floating Bodies*. J. Hydro. 22(2), 229-240 (2010).

[15] M.S. Longuet-Higgins, E.D. Cokelet: *The deformation of steep surface waves on water I: A numerical method of computation*. Proceedings of Royal Society, London 1976: 1-26.

[16] D.E.Nakos, D. Kring D, P.D. Sclavounos: *Rankine panel methods for transient free surface flows*. Proceedings of 6th International Conference on Numerical ship hydrodynamic, Iowa 1993: 251-269.

[17] D.Z. Ning, B. Teng: *Numerical simulation of fully nonlinear irregular wave tank in three dimensions*. Int. J. Numer. Meth. Fluids. 53, 1847–1862 (2007).

[18] D.Z. Ning, J. Zang, S.X. Liu, R.EatockTaylor, B. Teng, P.H. Taylor: *Free-surface evolution and wave kinematics for nonlinear uni-directional focused wave groups*. Ocean Eng. 36, 1226–1243 (2009).

[19] T.F. Ogilvie: *First- and second-order forces on a cylinder submerged under a free surface*. J. Fluid Mech. 16, 451–472 (1963).

[20] L. Piegl, W.Tiller: *The NURBS book*. 2nd ed. Springer, Germany (Berlin) 1990.

[21] S. Ryu, M.H. Kim, P.J. Lynett PJ: *Fully nonlinear wave-current interactions and kinematics by a BEM-based numerical wave tank*. Comput. Mech. 32, 336–346 (2003).

[22] H.J. Tang, C.C. Huang: *Bragg reflection in a fully nonlinear numerical wave tank based on boundary integral equation method*. Ocean Eng. 35, 1800-1810 (2008).

[23] K. Tanizawa: *A nonlinear simulation method of 3-D body motions in waves*. J. Soc. Nav. Arch. Japan. 178, 179-191 (1995).

[24] A. Tavassoli, M.H. Kim: *Interactions of fully non-linear waves with submerged bodies by a 2D Viscous NWT*. Proceedings of 11th International Offshore and Polar Engineering Conference, Stavanger 2001: Vol. 3, 348–354.

[25] T. Vinji, P. Brevig: *Numerical Simulation of breaking wave. Proceedings of 3rd International Finite Elements in Water Resources*, Oxford 1981: Vol. 5, 196-210.

[26] C.Z. Wang, G.X. Wu: *Interactions between fully nonlinear water waves and cylinder arrays in a wave tank*. Ocean Eng. 37, 400-417 (2010).

[27] C.Z. Wang, G.X.Wu: *Time domain analysis of second order wave diffraction by an array of vertical cylinders*. J. Fluids Struct. 23(4), 605-631 (2007).

[28] G.X. Wu, Z.Z. Hu: *Simulation of nonlinear interactions between waves and floating bodies through a finite-element-based numerical tank*. Proceedings of Royal Society, London 2004: 2797–2817.

[29] X.T. Zhang, B.C. Khoo, J. Lou: *Wave propagation in a fully nonlinear numerical wave tank: A desingularized method*. Ocean Eng. 33, 2310–2331 (2006).

Submitted: 12.11.2012

Accepted: 22.02.2013

Arash Abbasnia
Dr. Mahmoud Ghiasi
(Corresponding Author)
mghiasi@aut.ac.ir
Dept. of Maritime Engineering
Amirkabir University of Technology
424 Hafez Ave.
15875-4413 Tehran Iran